Journal of Magnetic Resonance **146,** 277–282 (2000)
doi:10.1006/jmre.2000.2149, available online at http://www.idealibrary.com on IDEAL®

Multiple-Quantum *J*-Resolved NMR Spectroscopy (MQ-JRES): Measurement of Multiple-Quantum Relaxation Rates and Relative Signs of Spin Coupling Constants

Maili Liu[1] and Xu Zhang

Laboratory of Magnetic Resonance and Atomic and Molecular Physics, Wuhan Institute of Physics and Mathematics, Chinese Academy of Sciences, Wuhan 430071, People's Republic of China

Received October 11, 1999; revised June 21, 2000

The technique of multiple-quantum *J*-resolved NMR spectroscopy (MQ-JRES) is introduced and applied to the spin system SI_3–M (such as in the example given here, the $^{13}CH_3$–^{12}CH in alanine). The SI_3 spin system was excited to its highest quantum state ($8S_yI_xI_yI_y$), which consists of four coherences: quadruple quantum of ($3I + S$), double quantum of ($3I - S$), double quantum of ($I + S$), and zero quantum of ($I - S$). In the MQ spectrum generated from the projection onto the F_1 dimension, the resonances of the different multiple-quantum coherences are resolved by their coupling constants to the remote spin (M). The absorptive lineshapes in both F_1 and F_2 dimensions enable accurate measurements of transverse relaxation rates, and both amplitude and relative signs of the long-range coupling constants are to be derived from either frequency or time domain data. The selective detection of MQ-JRES spectra of the individual MQ coherences using either phase cycling or pulsed field gradients is presented.

Key Words: **multiple quantum; relaxation times; *J*-resolved; coupling constant.**

INTRODUCTION

Multiple-quantum (MQ) coherences have been widely used in high-resolution NMR spectroscopy as a filter to simplify the spectrum or as a frequency modulator to create the second domain in a two-dimensional (2D) experiment. In addition, the relaxation rate of the MQ transition contains information on the spectral density function at the MQ frequency (*1–6*). Previous studies of MQ relaxation were mainly concerned with the case where all of the spins are involved in the MQ transition. Difficulties in the measurement of MQ relaxation rates include the effects of the remote coupling and the dispersive lineshape. These problems are, conventionally, avoided by using a specially chosen spin system, and an *n*-spin system, ideally with identical coupling constants, is normally chosen for the study of the *n*-quantum transition. Generally, the spin system is excited to its possible highest quantum order (n) using a pulse scheme of 90°–τ–90°, where the delay τ is set according to the coupling constants. The spin-echo sequence is applied to generate relaxation attenuation and, at the same time, to remove any chemical shift precession and field inhomogeneity. The experiment is normally carried out in a 2D manner with the MQ spectrum appearing in the F_1 dimension. The transverse relaxation rate of the MQ transition is established from the linewidth at half-height. The selective detection of a desirable MQ transition, especially a higher order one, requires intensive phase cycling, which is normally time consuming. General methods for the systematic design of phase cycle schemes have been described in detail (*5, 6*), and the TPPI method has been used successfully for separation of the MQ transitions (*7, 8*). Use of pulse field gradients (PFG) can greatly simplify the procedure and lead to higher selectivity at the expense of a loss of sensitivity (*9–11*). Furthermore, the effects of eddy currents and of molecular self-diffusion, both associated with the use of PFGs, can influence the accurate measurement of the relaxation rates.

We have described previously a method for enhancing the effect of the applied gradient strength using the MQ transitions of the $^{13}CH_3$ system, and applied this to self-diffusion coefficient measurement (*12*). The method is based on maximum-quantum filtering NMR spectroscopy (*13, 14*), and it is now modified here for the measurement of MQ relaxation rates of a $^{13}CH_3$ group in the CH_3–CH segment of the alanine molecule. It is shown that for the $^{13}CH_3$ system at the maximum-quantum status, a spin-echo experiment gives rise to a *m*ultiple-*q*uantum *J-res*olved spectrum (MQ-JRES). The MQ-JRES consists of four doublet splittings in the F_1 dimension corresponding to the MQ coupling constant combinations to the remote proton (in the CH moiety). This then enables accurate measurement of the linewidths or relaxation rate of the MQ transitions, as well as determining the amplitude and relative sign of the MQ coupling constants. The phase cycling program and ratios of the PFG strength for selective detection of individual MQ J-RES spectra are also presented.

[1] To whom correspondence should be addressed. Fax: 86-(0)27-87865291. E-mail: ml.liu@nmr.whcnc.ac.cn.

1090-7807/00 $35.00

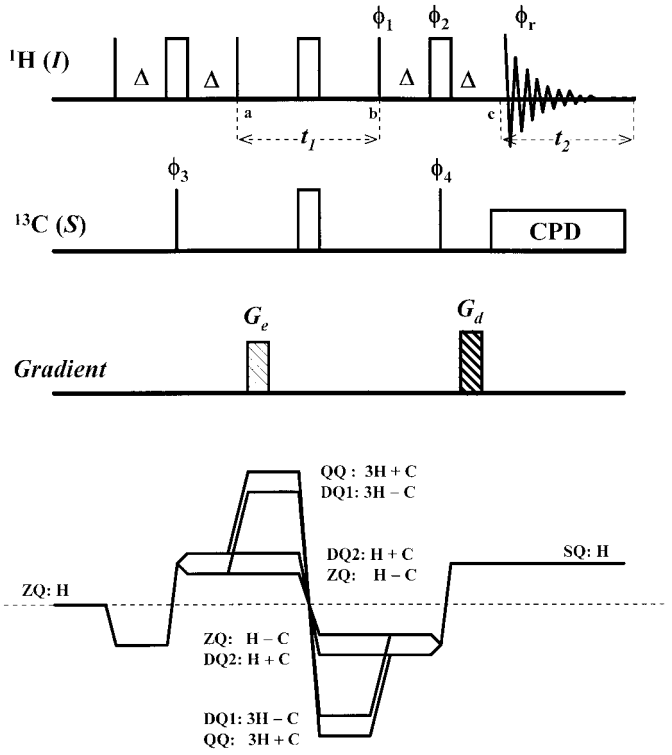

FIG. 1. Pulse sequence for *m*ultiple-*q*uantum *J-res*olved NMR spectroscopy (MQ-JRES) showing the coherence transfer pathways. Narrow and open bar symbols represent 90° and 180° pulses, respectively. The pulse field gradient pulses are shown using filled bar symbols. All pulses are applied along the *x* axis unless otherwise indicated. The phase cycling programs for selective detection are given in Table 1. Decoupling during the acquisition period is optimal.

PULSE SEQUENCE AND THEORY

The pulse sequence (Fig. 1) used in the experiment is similar to that used for the diffusion coefficient measurement (*12*). The modification is to insert two incremental times before and after the two π pulses in the middle of the pulse sequence. The detailed description of the MQ generation has been described previously (*13, 14*). We now focus on the analysis of the precession of the remote spin coupling, transverse relaxation, and the selective detection of the desired MQ coherence. For a spin system of SI_3-M (representing $^{13}CH_3$–^{12}CH in the alanine molecule), the pulse sequence generates a transverse spin operator of $8I_xI_yI_yS_y$ immediately before the evolution time (position a in Fig. 1). The operator gives rise to four different MQ transitions: quadruple quantum ($3I + S$, QQ), double quanta ($3I - S$, DQ1) and ($I + S$, DQ2), and zero quantum ($I - S$, ZQ).

Since all of the spins in the SI_3 system are involved in the transverse operator ($8I_xI_yI_yS_y$), there is no direct coupling ($^1J_{IS}$). Simultaneously application of the two 180° pulses on spins I and S in the middle of the evolution time refocuses all chemical shift ($\omega_{I,S}$) precessions, removes field inhomogeneity, and, more importantly, ensures no interchange of the multiple-quantum coherences during the t_1 period. However, the remote J couplings of the spins I and S with the spin M (denoted $^3J_{IM}$ and $^2J_{SM}$) and the transverse relaxation remain active. At the end of the incremental period (position b in Fig. 1), the observable terms may be written as

$$\begin{aligned}
\sigma_1 &= \Sigma\sigma(\mathrm{MQ}) \\
&= \sigma(\mathrm{QQ}) + \sigma(\mathrm{DQ1}) + \sigma(\mathrm{DQ2}) + \sigma(\mathrm{SQ}) \qquad [1a]\\
\sigma(\mathrm{QQ}) &= (3I_xI_yI_yS_y - 3I_xI_xI_yS_x - I_xI_xI_xS_y + I_yI_yI_yS_x) \\
&\quad \times \cos[\pi(3J_{IM} + J_{SM})t_1]\exp[-t_1/T_{2\mathrm{QQ}}] \qquad [1b]\\
\sigma(\mathrm{DQ1}) &= (3I_xI_yI_yS_y + 3I_xI_xI_yS_x - I_xI_xI_xS_y - I_yI_yI_yS_x) \\
&\quad \times \cos[\pi(3J_{IM} - J_{SM})t_1]\exp[-t_1/T_{2\mathrm{DQ1}}] \qquad [1c]\\
\sigma(\mathrm{DQ2}) &= (I_xI_yI_yS_y + I_xI_xI_yS_x + I_xI_xI_xS_y + I_yI_yI_yS_x) \\
&\quad \times \cos[\pi(J_{IM} + J_{SM})t_1]\exp[-t_1/T_{2\mathrm{DQ2}}] \qquad [1d]\\
\sigma(\mathrm{ZQ}) &= (I_xI_yI_yS_y - I_xI_xI_yS_x + I_xI_xI_xS_y - I_yI_yI_yS_x) \\
&\quad \times \cos[\pi(J_{IM} - J_{SM})t_1]\exp[-t_1/T_{2\mathrm{ZQ}}]. \qquad [1e]
\end{aligned}$$

After the mixing scheme of $-90_{\phi 1}(I)-\Delta-180_{\phi 2}(I)90_{\phi 4}(S)-\Delta-$ the detectable signals become (position c in Fig. 1)

$$\begin{aligned}
\sigma_{2\mathrm{MQ}} &= k[I_y\cos(2\phi_2 - \phi_1) - I_x\sin(2\phi_2 - \phi_1)] \\
&\quad \times \cos(\Phi_{\mathrm{MQ}})\cos(\pi J_{\mathrm{MQ}}t_1)\exp(-t_1/T_{2\mathrm{MQ}}). \qquad [2]
\end{aligned}$$

The parameters for the four multiple-quantum coherences are defined as

$$\begin{aligned}
&\mathrm{QQ}: k = 3/8; \quad \Phi_{\mathrm{MQ}} = 3\phi_1 + \phi_4; \quad J_{\mathrm{MQ}} = 3J_{IM} + J_{SM};\\
&\mathrm{DQ1}: k = 3/8; \quad \Phi_{\mathrm{MQ}} = 3\phi_1 - \phi_4; \quad J_{\mathrm{MQ}} = 3J_{IM} - J_{SM};\\
&\mathrm{DQ2}: k = 1/8; \quad \Phi_{\mathrm{MQ}} = \phi_1 + \phi_4; \quad J_{\mathrm{MQ}} = J_{IM} + J_{SM};\\
&\mathrm{ZQ}: k = 1/8; \quad \Phi_{\mathrm{MQ}} = \phi_1 - \phi_4; \quad J_{\mathrm{MQ}} = J_{IM} - J_{SM}.
\end{aligned} \qquad [3]$$

It should be noted that for the MQ coherences, the composition of a coupling constant combination (J_{MQ}) and the phase factor (Φ_{MQ}), as well as the effective chemical shift and PFG-induced phase-shift (*12*), are identical to, and depend on, the composition of the MQ coherence. When $(2\phi_2 - \phi_1)$ is kept constant at 0 or π, only the terms containing I_y gives rise to NMR signals and the expression in Eq. [2], $\sigma_{2\mathrm{MQ}}$, is simplified to

$$\begin{aligned}
\sigma_2 = (1/8)I_y[&3\cos(\pi J_{\mathrm{QQ}}t_1)\exp(-t_1/T_{2\mathrm{QQ}}) \\
&+ 3\cos(\pi J_{\mathrm{DQ1}}t_1)\exp(-t_1/T_{2\mathrm{DQ1}}) \\
&+ \cos(\pi J_{\mathrm{DQ2}}t_1)\exp(-t_1/T_{2\mathrm{DQ2}}) \\
&+ \cos(\pi J_{\mathrm{ZQ}}t_1)\exp(-t_1/T_{2\mathrm{ZQ}})]. \qquad [4]
\end{aligned}$$

Equation [4] implies absorptive lineshapes in both F_1 and F_2 dimensions after the 2D Fourier transformation. This should be

TABLE 1
Phase Cycling Programs for Nonselective and Selective Detected MQ-JRES

Pulse phases	Nonselective	QQ ($3I + S$)	DQ1 ($3I - S$)	DQ2 ($I + S$)	ZQ ($I - S$)
ϕ_1	0°	15°, 135°, 255°	15°, 135°, 255°	15°, 255°	15°, 255°
ϕ_2	0°	7.5°, 67.5°, 127.5°	7.5°, 67.5°, 127.5°	7.5°, 127.5°	7.5°, 127.5°
ϕ_3	0°, 180°	6(0°), 6(180°)	6(0°), 6(180°)	4(0°), 4(180°)	4(0°), 4(180°)
ϕ_4	0°, 0°, 180°, 180°	3(135°), 3(315°)	3(45°), 3(225°)	2(135°), 2(315°)	2(45°), 2(225°)
ϕ_r	0°, 180°, 180°, 0°	3(0°), 6(180)°, 3(0°)	3(0°), 6(180)°, 3(0°)	180°, 0°, 0°, 180°, 0°, 180°, 180°, 0°	0°, 180°, 180°, 0°, 80°, 0°, 0°, 180°

very useful for accurate measurements of the spin coupling constants and the transverse relaxation rates of the MQ transitions. The selective detected MQ-JRES spectrum can be achieved by cycling the phases ϕ_1 and ϕ_4 according to Eqs. [2] and [3]. The general phase program is given in Table 1. Alternatively, the use of PFG can provide a more effective way of obtaining separated MQ-JRES spectra. In the simplest case, the MQ coherence-encoding gradient (G_e) may be applied during the evolution period and the decoding gradient pulse (G_d) before data acquisition. After considering the effect of the PFG, the observable term becomes

$$\sigma_{3MQ} = I_y \cos(\Phi_{MQ})\cos(\psi_{MQ} + \gamma_H G_d \delta) \times \cos(\pi J_{MQ} t_1)\exp(-t_1/T_{2MQ}), \quad [5]$$

where $\Psi_{MQ} = \gamma_{MQ} G_e \delta$ represents the rotation angle induced by the gradient pulse, and γ_{MQ} is the effective gyromagnetic ratio and is defined as $(3\gamma_H + \gamma_C)$, $(3\gamma_H - \gamma_C)$, $(\gamma_H + \gamma_C)$, and $(\gamma_H - \gamma_C)$ for the QQ, DQ1, DQ2, and ZQ coherences, respectively. G and δ are the gradient strength and duration. For selective detection, the required gradient strength ratios of G_e:G_d are −8:26 for QQ, −8:22 for DQ1, −8:10 for DQ2, and −8:6 for ZQ if the shape and the duration of the PFG pulses are the same. However, application of PFGs for the MQ coherence selection can lead to a sensitivity loss and can also increase the relaxation rates because of the eddy currents induced by gradient pulse. It should be stated that the use of PFG as depicted in the pulse sequence requires back-prediction of the t_1 interferograms due to the finite width of the encoding gradient (G_e).

The MQ coupling constants and the transverse-relaxation times can be obtained directly from the splittings and the half linewidth in the F_1 dimension of the MQ-JRES spectra, respectively. More accurate measurements can be achieved by fitting the time domain data to Eq. [4]. For this purpose, the selective detected MQ-JRES spectra can greatly simplify the procedure.

EXPERIMENTAL

The test sample was 30 mg alanine (Shanghai Kongda, China) in 0.5 ml D_2O. The spin system was therefore SI_3M, representing $^{13}CH_3$–^{12}CH in the alanine molecule at natural abundance. The coupling constants $^1J_{SI}$, $^2J_{SM}$, and $^3J_{IM}$ are 139.7, 4.52, and 7.27 Hz, respectively, as obtained from the high-resolution 1D NMR spectra.

All experiments were carried out using a Bruker ARX500 spectrometer with a gradient unit capable of delivering a *z*-field gradient up to 49 mT/m. The operating frequencies for ^{1}H and

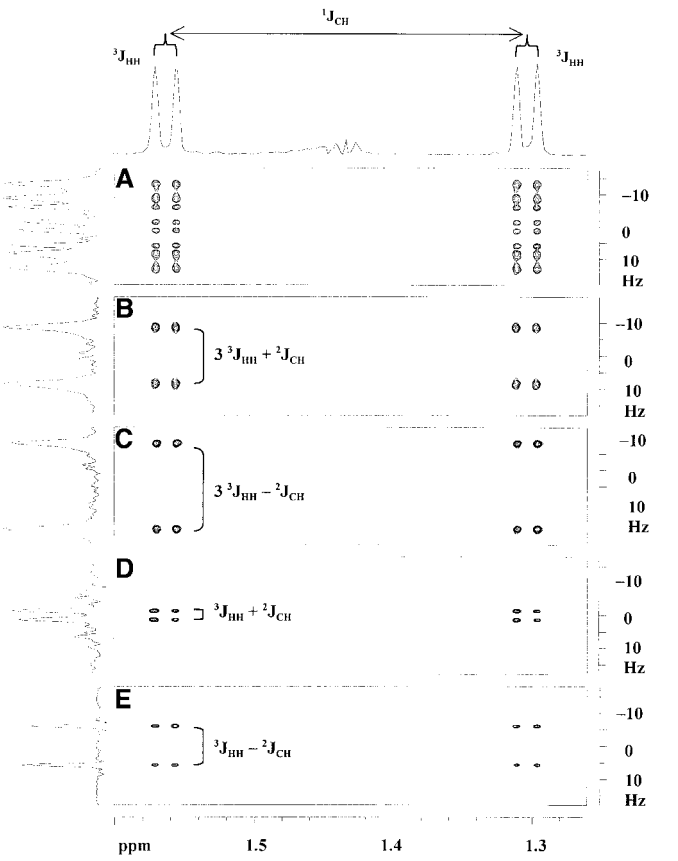

FIG. 2. Multiple-quantum *J*-resolved NMR spectra of a $^{13}CH_3$ group in an SI_3-M spin system obtained by (A) nonselective and (B) selective detection of the quadruple-quantum ($3I + S$), (C) double-quantum ($3I - S$), (D) double-quantum ($I + S$), and (E) zero-quantum ($I - S$) coherences. The projection in F_2 shows the ^{1}H NMR spectrum of the methyl group protons with the signal from $^{12}CH_3$ protons being suppressed. The projection into the F_1 dimension represents the corresponding MQ spectrum and is given at the left side of the 2D plot.

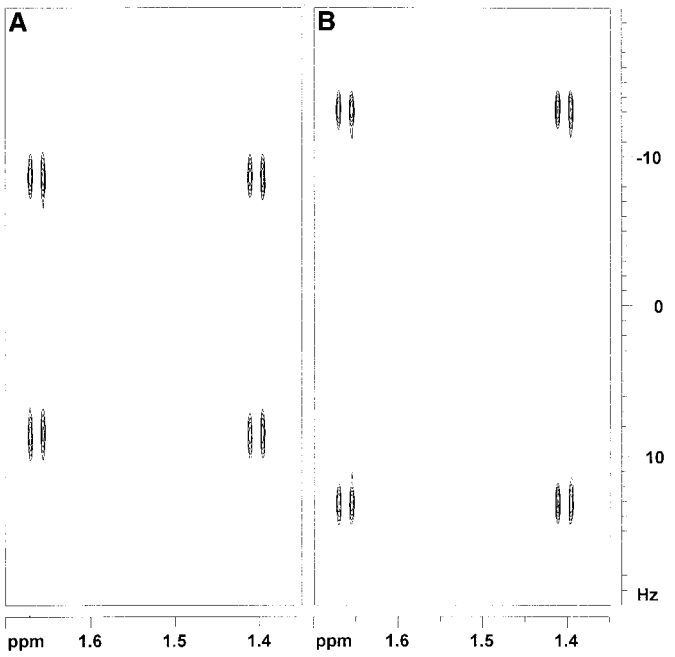

FIG. 3. PFG-selected (A) quadruple-quantum ($3I + S$) and (B) double-quantum ($3I - S$) J-resolved NMR spectra. The smaller splitting of the QQ transition indicates the opposite relative signs of the long-range coupling constants, $^2J_{CH}$ and $^3J_{HH}$.

^{13}C were 500.13 and 125.76 MHz, respectively. The pulse sequence and the coherence transfer pathways used in the experiment are shown in Fig. 1. A BIRD (*15*) approach followed by a recovery delay of 0.5 s was used before the main part of the pulse sequence to suppress the signals of $^{12}CH_n$ groups. The delay (Δ) was set to 3.58 ms corresponding to $^1J_{IS}$ of 139.7 Hz. The spectral widths were 100 and 1000 Hz in the F_1 and F_2 dimensions, respectively. Typically, 16 transients were co-added into 1024 complex data points in the F_2 dimension without decoupling during the acquisition. A total of 128 increments were acquired in the F_1 dimension using the phase-sensitive mode of the standard Bruker QSEQ method. A $\pi/2$ phase-shifted sine-shaped window function was applied in F_2 before Fourier transformation, and there was no weighting in the F_1 dimension in order not to affect the lineshapes in that dimension. The phase programs listed in Table 1 were used for nonselective and selective measurements.

A 1-ms sine-shaped gradient pulse was used for the PFG-selected experiments. The encoding and decoding gradient strengths (G_e:G_d in units of mT/m:mT/m) were -8:26 for QQ, -8:22 for DQ1, -8:10 for DQ2, and -8:6 for ZQ. An extra delay of 1 ms is required in the last part of t_1 if the gradient pulse is used.

RESULTS AND DISCUSSION

MQ-JRES spectroscopy. Figure 2 shows nonselective (Fig. 2A) and a series of selective (Figs. 2B–2E) MQ-JRES spectra of the $^{13}CH_3$ protons in the SI_3–M spin system, where the large splitting (139.7 Hz) in the F_2 dimension is caused by the one-bond coupling constant ($^1J_{IS}$). The MQ spectrum obtained from the projection into the F_1 dimension is given at the left side of the corresponding 2D plot. Although $8I_xI_yI_yS_y$ is a single operator, it contains four MQ transitions as described by Eq. [1] in the previous section. Each MQ transition shows a different combination of spin coupling to the remote proton (spin M), which results in four, well-resolved doublets in the nonselective MQ-JRES spectrum (Fig. 2A) representing the resonances of the four MQ coherences. The measured intensity ratios of the MQ peaks are 3.1:2.9:1.1:0.9 (QQ:DQ1:DQ2:ZQ), close to the theoretical ratios of 3:3:1:1. Using the phase program listed in Table 1, the selective MQ-JRES spectra of the individual MQ coherences are obtained and show in Figs. 2B–2E, in which the composition of the MQ coupling constants are labeled.

In the individual MQ-JRES spectra, J(QQ) (Fig. 2B) is smaller than J(DQ1) (Fig. 2C), and J(DQ2) (Fig. 2D) is smaller than J(ZQ) (Fig. 2E). These is a result of the opposite signs of the coupling constant, $^2J_{SM}$, to that of $^3J_{IM}$ (assumed positive) (*16*). The negative sign of $^2J_{SM}$ is confirmed by the gradient-selected QQ-JRES (Fig. 3A) and DQ1-JRES (Fig. 3B) spectra. Referring to Eq. [3], it is possible to derive the values

TABLE 2
Multiple Quantum Relaxation Rates and Linewidths at Half-Height Obtained from the Nonselective and Selective (Sel-) MQ-JRES Measurements

Name	QQ (3H + C)	DQ (3H − C)	DQ2 (H + C)	ZQ (H − C)
Peak Area ± Std[a]	3.10 ± 0.10	2.94 ± 0.08	1.09 ± 0.05	0.86 ± 0.05
R_2 ± Std (s^{-1})[a]	7.01 ± 0.30	6.04 ± 0.22	1.84 ± 0.21	1.26 ± 0.19
$\nu_{1/2}$ (Hz)	2.64 ± 0.12	2.25 ± 0.12	1.30 ± 0.12	1.09 ± 0.12
R_2 ± Std (s^{-1})	8.29 ± 0.38	7.07 ± 0.38	4.08 ± 0.38	3.42 ± 0.38
Sel-R_2 ± Std (s^{-1})[a]	7.56 ± 0.15	6.19 ± 0.13	2.14 ± 0.34	1.21 ± 0.29
Sel-$\nu_{1/2}$ (Hz)	2.35 ± 0.12	1.97 ± 0.12	1.00 ± 0.12	0.93 ± 0.12
Sel-R_2 ± Std (s^{-1})	7.38 ± 0.38	6.19 ± 0.38	3.14 ± 0.38	2.92 ± 0.38

[a] Obtained from fitting the time domain data to Eq. [2].

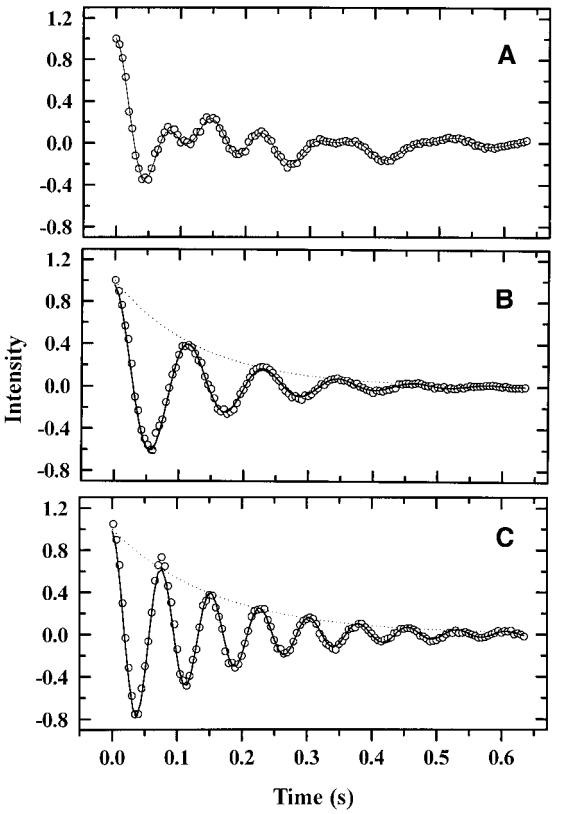

FIG. 4. Time domain signal evolutions (open-circle symbols) in the (A) nonselective, (B) quadruple-quantum ($3I + S$), and (C) double-quantum ($3I - S$) selective MQ-JRES experiments. The MQ transverse-relaxation rates and the coupling constants to the remote proton are revealed by fitting experimental data to Eq. [4] (solid line). The dotted line in (B) and (C) represents the MQ relaxation curve.

of the scalar coupling constants of $^2J_{SM}$ and $^3J_{IM}$ from the combination of any of the two MQ coupling constants. The method thus provides an alternative way of determining the sign and amplitudes of the long-range coupling constants. The values of J_{IM} and J_{SM} are 7.20 ± 0.15 and −4.51 ± 0.15 Hz, derived from the nonselective MQ-JRES spectrum, and 7.24 ± 0.15 and −4.52 ± 0.15 Hz from the selective experiments, respectively. These values agree with the coupling constants of 7.27 and −4.52 Hz measured directly from the 1D spectra.

It is not surprising to find that the spectral linewidths at half-height ($\nu_{1/2}$) of the MQ transitions are, as expected, in the order of $\nu_{1/2}(\mathrm{QQ}) > \nu_{1/2}(\mathrm{DQ1}) > \nu_{1/2}(\mathrm{DQ2}) > \nu_{1/2}(\mathrm{ZQ})$. The linewidth can be converted into the transverse-relaxation rate according to $R_2 = \pi\nu_{1/2}$. The results are listed in Table 2.

Measurement of the R_{2MQ} and ^nJ using the time domain data. The time domain NMR data can also be used for the measurements of $R_{2\mathrm{MQ}}$, $^2J_{\mathrm{SM}}$, and $^3J_{\mathrm{IM}}$. As described in Eq. [4], the nonselective signal consists of four components corresponding to the four MQ coherences. Each component is modulated by a characteristic frequency (J_{MQ}) and by an attenuation factor ($R_{2\mathrm{MQ}}$). Figure 4 shows the time domain signal evolution (open-circle symbols), also known as the free-induction decay (FID), of the SI_3 system during the t_1 period in nonselective (Fig. 4A), QQ-selective (Fig. 4B), and DQ1-selective (Fig. 4C) experiments. The solid lines represents the fitting of the time domain signals to Eq. [4]. The dotted lines in Figs. 4B and 4C indicate the relaxation decay of the corresponding MQ transition. The parameters derived from the fitting are listed in Table 2. The excellent match between the experimental data and the theoretical fit is demonstrated in Fig. 4 and Table 2.

It can be seen from Table 2 that the transverse-relaxation rates established from the linewidth analysis are larger than those from the time domain data in the nonselective experiment. The difference becomes significant when the effective quantum order becomes smaller. This may be caused by data truncation since the evolution time in the F_1 dimension is only 635 ms. The selective measurements result in a much better agreement with relaxation rates obtained from the frequency and time domain data and, at the same time, greatly simplify the fitting procedure because of the unit single-frequency modulation (J_{MQ}) and monoexponential decay ($R_{2\mathrm{MQ}}$, dotted line). The $^3J_{IM}$ value of 7.25 ± 0.01 Hz and $^2J_{SM}$ value of −4.57 ± 0.02 Hz obtained from the fitting are very close to those determined from the 1D and 2D MQ-JRES spectra.

SUMMARY

Two-dimensional MQ-JRES NMR spectroscopy is presented and used for measuring the transverse-relaxation rates of the MQ transitions by either frequency or time domain data analysis. The method can also be applied, as an alternative method, to determine the amplitude and sign of the long-range hetero- and homonuclear coupling constants. In the nonselective experiment, the resonances of different MQ transitions are resolved by their effective coupling constants to the remote proton. This straightforwardly results in a high-resolution NMR spectrum of the MQ coherences from projection into the F_1 dimension with a two-step phase cycling at the minimum. The selective MQ-JRES approach is useful in simplifying the spectrum and in increasing the accuracy of the measurement of the parameters mentioned above. The phase program and the gradient strength ratios for obtaining the selective MQ-JRES spectrum are presented.

ACKNOWLEDGMENTS

This work is supported by the grants from the National Natural Science Foundation of China (NSFC 29925515 and 29875034) and the Chinese Academy of Sciences (KJ951-B1-402). The authors are grateful to Professor John C. Lindon for reading and editing the manuscript.

REFERENCES

1. M. E. Stoll, A. J. Vega, and R. W. Vaughan, Double resonance interferometry: Relaxation times for dipolar forbidden transitions and off-resonance effects in an AX spin system, *J. Chem. Phys.* **67,** 2029 (1977).
2. A. Wokaun and R. R. Ernst, The use of multiple quantum transitions for relaxation studies in coupled spin system, *Mol. Phys.* **36,** 317–341 (1978).
3. J. Tang and A. Pines, Multiple quantum NMR and relaxation of an oriented CH_3 group, *J. Chem. Phys.* **72,** 3290–3297 (1980).
4. R. R. Ernst, G. Bodenhausen, and A. Wokaun, "Principles of Nuclear Magnetic Resonance in One and Two Dimensions," Clarendon Press, Oxford (1987).
5. G. Bodenhausen, H. Kogler, and R. R. Ernst, Selection of coherence-transfer pathways in NMR pulse experiments, *J. Magn. Reson.* **58,** 370–388 (1984).
6. L. Braunschweiler, G. Bodenhausen, and R. R. Ernst, Analysis of networks of coupled spins by multiple quantum NMR, *Mol. Phys.* **48,** 535–560 (1983).
7. G. Bodenhausen, R. L. Vold, and R. R. Vold, Multiple quantum spin-echo spectroscopy, *J. Magn. Reson.* **37,** 93–106 (1980).
8. D. Drobny, A. Pines, S. Sinton, D. Weitekamp, and D. Wemmer, Fourier transform multiple quantum nuclear magnetic resonance, *J. Faraday Div. Chem. Soc. Symp.* **13,** 49–55 (1979).
9. A. A. Maudsley, A. Wokaun, and R. R. Ernst, Coherence transfer echoes, *Chem. Phys. Lett.* **55,** 9–14 (1978).
10. A. Bax, P. G. de Jong, A. F. Mehilkopf, and J. Smidt, Separation of the different orders of NMR multiple-quantum transitions by the use of pulsed field gradients, *Chem. Phys. Lett.* **69,** 567–570 (1980).
11. J. Ruiz-Cabello, G. W. Vuister, C. T. W. Moonen, P. Van Gelderen, J. S. Cohn, and P. C. M. Van Zijl, Gradient-enhanced heteronuclear correlation spectroscopy, theory and experimental aspects, *J. Magn. Reson.* **100,** 282–302 (1992).
12. M. L. Liu, X. A. Mao, C. H. Ye, J. K. Nicholson, and J. C. Lindon, Enhanced effect of magnetic field gradients using multiple quantum NMR spectroscopy applied to self-diffusion coefficient measurement, *Mol. Phys.* **93,** 913–920 (1998).
13. M. L. Liu, R. D. Farrant, J. K. Nicholson, and J. C. Lindon, Selective detection of ^{1}H NMR resonance of $^{13}CH_n$ groups using a heteronuclear maximum-quantum filter and pulsed field gradients, *J. Magn. Reson. B* **106,** 270–278 (1995).
14. M. L. Liu, R. D. Farrant, J. K. Nicholson, and J. C. Lindon, Selective Detection of ^{1}H NMR resonance of $^{13}CH_n$ groups using two-dimensional maximum-quantum correlation spectroscopy, *J. Magn. Reson. A* **112,** 208–219 (1995).
15. J. R. Garbow, D. P. Weitekamp, and A. Pines, Bilinear rotation decoupling of homonuclear scalar interactions, *Chem. Phys. Lett.* **93,** 504–509 (1982).
16. J. L. Marshall, "Carbon–Carbon and Carbon–Proton NMR Couplings: Applications to Organic Stereochemistry and Conformational Analysis," Verlag Chemie International, Florida (1983).